Real-Space Transmission Electron: Microscopy Investigations of Attachment of Functionalized Magnetic Nanoparticles to DNA-Coils Acting as a Biosensor

ARTICLE *in* THE JOURNAL OF PHYSICAL CHEMISTRY B · OCTOBER 2010

Impact Factor: 3.3 · DOI: 10.1021/jp105756b · Source: PubMed

9 AUTHORS, INCLUDING:

Teresa Zardán Gómez de la Torre
Uppsala University
16 PUBLICATIONS **195** CITATIONS
SEE PROFILE

Klas Gunnarsson
Uppsala University
50 PUBLICATIONS **655** CITATIONS
SEE PROFILE

Peter Svedlindh
Uppsala University
278 PUBLICATIONS **5,466** CITATIONS
SEE PROFILE

Maria Strømme
Uppsala University
226 PUBLICATIONS **3,973** CITATIONS
SEE PROFILE

Real-Space Transmission Electron Microscopy Investigations of Attachment of Functionalized Magnetic Nanoparticles to DNA-Coils Acting as a Biosensor

Sultan Akhtar,[†] Mattias Strömberg,[‡] Teresa Zardán Gómez de la Torre,[‡] Camilla Russell,[§] Klas Gunnarsson,[∥] Mats Nilsson,[§] Peter Svedlindh,*[,∥] Maria Strømme,*[,‡] and Klaus Leifer*[,†]

Department of Engineering Sciences, Division of Electron Microscopy and Nanoengineering, Department of Engineering Sciences, Division of Nanotechnology and Functional Materials, and Department of Engineering Sciences, Division of Solid State Physics, The Ångström Laboratory, Uppsala University, Box 534, SE-751 21 Uppsala, Sweden, and Department of Genetics and Pathology, Rudbeck Laboratory, Uppsala University, SE-751 85 Uppsala, Sweden

Received: June 22, 2010; Revised Manuscript Received: August 17, 2010

The present work provides the first real-space analysis of nanobead−DNA coil interactions. Immobilization of oligonucleotide-functionalized magnetic nanobeads in rolling circle amplified DNA-coils was studied by complex magnetization measurements and transmission electron microscopy (TEM), and a statistical analysis of the number of beads hybridized to the DNA-coils was performed. The average number of beads per DNA-coil using the results from both methods was found to be around 6 and slightly above 2 for samples with 40 and 130 nm beads, respectively. The TEM analysis supported an earlier hypothesis that 40 nm beads are preferably immobilized in the interior of DNA-coils whereas 130 nm beads, to a larger extent, are immobilized closer to the exterior of the coils. The methodology demonstrated in the present work should open up new possibilities for characterization of interactions of a large variety of functionalized nanoparticles with macromolecules, useful for gaining more fundamental understanding of such interactions as well as for optimizing a number of biosensor applications.

1. Introduction

Medicine, molecular biology, and other life science areas require biosensing technologies for detection of, for example, single-stranded DNA, proteins, or antibodies that are simple, sensitive, rapid, and inexpensive.[1] Traditional biosensors relying on nonmagnetic transduction mechanisms typically use fluorescent, electrochemical, or optical analytical tools. These offer a number of advantages but are also often connected with limitations such as, for example, expensive instrumentation and time-consuming sample preparations.[2−4] A large variety of biosensors that are currently under development make use of nanoparticles that are functionalized and operate in an environment of biomolecules. Moreover, the use of nanomaterials in biosensing applications and the design of biosensors on nanoscale dimensions offer a large number of advantages and have become more common in biosensor research.[5,6] In particular, the use of magnetic micro- and nanoparticles (magnetic beads) in biosensing applications offers unique properties, because there is no magnetic background in most biological samples.[7] Furthermore, beads are rather inexpensive to produce, can easily be biofunctionalized, and are physically and chemically stable. Magnetic biosensors can be categorized as either substrate-based (magnetic biochip technology) or substrate-free (lab-on-a-bead technology). In the former category, if the target molecule is present, the biofunctionalized magnetic beads bind to the sensor surface and induce a signal change.[8,9] The latter sensor type measures the change of magnetic bead properties, most commonly the magnetic relaxation time.[10,11] Any sensor capable of measuring the magnetic field from magnetic beads can be used both in substrate-based and substrate-free sensor platforms.

To develop optimal biosensors using nanoparticles, the details of the interaction and attachment of the nanoparticles with molecules must be understood. Though, in principle, structural and chemical order in biological nanoparticles can be visualized,[12] to date, there is only a limited range of analysis methodologies available to study such functionalization and interactions in real-space.

Recently, we provided a proof-of-principle of a novel substrate-free magnetic DNA bioassay suitable as a platform for low-cost and easy-to-use diagnostic devices: the volume-amplified magnetic nanobead detection assay (VAM-NDA).[13,14] This biosensor principle is based on the base-pair hybridization of oligonucleotide-functionalized magnetic beads to DNA-coils formed by rolling circle amplification (RCA) in solution (bead immobilization). Because the oligonucleotide-functionalized magnetic beads are only immobilized if the oligonucleotide is complementary to the sequence of the DNA-coil, the bead-coil interaction is highly sequence specific.[13] The read-out is performed by measuring the sample response in an oscillating magnetic field. Details of the assay as well as descriptions of the underlying magnetic theory are given in earlier work.[13,15−19]

The main aim of the present study is to create a methodology to study the interaction between DNA-functionalized magnetic nanoparticles and DNA macromolecules in real-space using transmission electron microscopy (TEM). Moreover, we provide a first-time TEM visualization of magnetic beads hybridized to DNA-coils, and the affinity of two differently sized beads (40

* Corresponding authors. Telephone: +46 (0)18-471 3135, fax: +46 (0)18-471 3270, e-mail: peter.svedlindh@angstrom.uu.se (P.S.); telephone: +46 (0)18-471 7231, e-mail: maria.stromme@angstrom.uu.se (M.S.); telephone: +46 (0)18-471 7942, e-mail: klaus.leifer@angstrom.uu.se (K.L.).

[†] Department of Engineering Sciences, Division of Electron Microscopy and Nanoengineering.

[‡] Department of Engineering Sciences, Division of Nanotechnology and Functional Materials.

[§] Department of Genetics and Pathology.

[∥] Department of Engineering Sciences, Division of Solid State Physics.

10.1021/jp105756b
Published on Web 09/27/2010

and 130 nm) to nonstained and unlabeled DNA-coils are described. The findings from the TEM characterization are compared with the results from the magnetic characterization of similar samples.

2. Experimental Section

2.1. Oligonucleotide Functionalization of Magnetic Beads and Synthesis of DNA-Coils. Two aqueous suspensions of relatively monodisperse amino group-modified magnetic nanobeads (maghemite, nanomag-D NH_2) having nominal sizes of 40 and 130 nm, respectively, were supplied from Micromod Partikeltechnologie, Germany. Thiolated and fluorescence-labeled oligonucleotides (SH-5′-TTTTTTTTTTTTTTTTTTTTT-GTTGATGTCATGTGTCGCAC-3′-FITC) were conjugated to each bead type using SPDP chemistry, giving two batches (carrier liquid 1 × PBS (pH 7.4), 137 mM NaCl, 2.7 mM KCl, 8.1 mM $Na_2HPO_4 \cdot 2H_2O$, 1.47 mM KH_2PO_4) of functionalized beads; a 40 nm bead batch (three oligonucleotides per bead, 1.29×10^{13} beads per mL) and a 130 nm bead batch (two oligonucleotides per bead, 6.77×10^{11} beads per mL). Detailed functionalization protocols are given in previous works,[13,16] and the oligonucleotide surface coverage was analyzed using a fluorescence-based approach.[13] Judging from the polydispersity indices (PDIs) obtained from dynamic light scattering measurements on oligonucleotide-functionalized 40 and 130 nm sized beads without DNA-coils (PDI 0.14 and 0.098, respectively), individual beads are in majority in solution.[18]

The procedures for target recognition (padlock sequence 5′-TAGGTTGAGCCCAGGGACTTCTAGAGTGTACCGAC-CTCAGTAGCCGTGACTATCGACTTGTTGATGTCATGTG-TCGCACCAAATGCGATTCC-3′, target sequence 5′-CCCT-GGGCTCAACCTAGGAATCGCATTTG-3′) and RCA are described elsewhere.[13] An RCA-time of 1 h was employed which resulted in RCA-coils having a hydrodynamic diameter of about 700 nm[13,20] and where the total length of the 90 000 base-pair DNA single-strand was about 30 μm, assuming an enzymatic amplification rate of 1500 nucleotides per min.[21]

2.2. Magnetic Characterization. A 25 μL amount of bead batch solution was mixed with 25 μL of a solution with a given concentration of DNA-coils (0 pM to 600 pM; 0 pM refers to a negative control sample) and 10 ng/μL genomic background derived from a blood sample of a human male individual. A 30 μL amount of the mixture was extracted for immediate characterization in a Superconducting Quantum Interference Device magnetometer (QD MPMS XL, Quantum Design). The characterization began with 30 min of incubation at 70 °C; thereafter, the complex magnetic moment was measured at 37 °C (frequency range 10 to 1000 Hz, AC excitation field amplitude 2 Oe). Finally, the saturation magnetic moment was determined at 37 °C in order to obtain the complex magnetization (given as mass magnetization, with mass referring to weight of magnetic beads) and for calculating the magnetic bead concentration (diamagnetic contribution from sample holder subtracted). It was not practically possible to use the same concentration of 40 nm beads as for 130 nm beads because of the comparably very low magnetic moment of the 40 nm beads. In fact, the SQUID magnetometer would have been unable to record the complex magnetic moment of samples with such a low concentration of 40 nm beads.

2.3. TEM Sample Preparation and Characterization. Three different samples were prepared (genomic background material excluded): a negative control sample containing no DNA-coils based on the 130 nm bead batch and positive samples based on the 130 and 40 nm bead batches. The first sample was prepared by mixing 5 μL of 130 nm bead batch solution and 5 μL of hybridization buffer, pH 8 (40 mM Tris-HCl ($C_4H_{11}NO_3 \cdot HCl$), 40 mM EDTA ($C_{10}H_{16}N_2O_8$), 0.2 v/v % Tween-20 ($C_{58}H_{114}O_{26}$), and 1 M NaCl) in an Eppendorf tube followed by incubation at 70 °C for 30 min and thereafter addition of 990 μL of 1 × PBS. The second sample was prepared in the same way as the first except for adding 5 μL of DNA-coil solution (200 pM DNA-coils, 40.01 mM Tris-HCl, 40 mM EDTA, 0.27 v/v % Tween-20, 1 M NaCl, 0.002 mM $MgCl_2$, 0.001 mM DTT ($C_4H_{10}O_2S_2$), 0.002 μM spermidine ($C_7H_{19}N_3$), 20.13 mM Tris-acetate ($C_4H_{11}NO_3 \cdot C_2H_4O_2$), 6.1 mM Mg-acetate ($C_4H_6MgO_4$), 40.26 mM K-acetate ($C_2H_3KO_2$)) instead of 5 μL of hybridization buffer. The third sample was prepared in the same way as the second except for using 40 nm bead batch solution and adding 90 μL of 1 × PBS after incubation. Detailed compositions of the prepared sample solutions are given in Supporting Information. It should be noted that the ratios between the total number of beads and DNA-coils for both positive samples prepared for TEM are the same as for the samples with 100 pM DNA-coil concentration prepared for magnetic measurements. Because it is reasonable to assume that the dilution with 1 × PBS does not significantly affect the attachment of beads to DNA-coils, the positive samples for TEM and magnetic measurements can be considered as equivalent with respect to the distribution of immobilized beads in the DNA-coils.

The TEM samples were prepared by dropping a small amount of each of the prepared samples onto the amorphous holey carbon support films followed by drying of the droplets in open air. The grids were thereafter installed and studied by bright-field imaging (acceleration voltage 200 kV) in a JEOL 2000FXII TEM.

3. Results and Discussion

Figure 1 displays the imaginary part of the complex magnetization (m'') vs frequency recorded at 37 °C for samples containing 40 nm beads (panel a) and 130 nm beads (panel b) at various DNA-coil concentrations. In both panels, the peak height decreases with increasing DNA-coil concentration as expected since the number of immobilized beads increases. As found earlier,[13] the observed peak height is in fact directly proportional to the number of nonimmobilized beads. Thus, in particular, for the samples with 100 pM DNA-coil concentration, the total number of immobilized beads equals the total number of beads multiplied by y/x where y and x are defined in Figure 1. From this information, we find that the average number of immobilized beads per DNA-coil for a 100 pM concentration of DNA-coils in Figure 1 equals 5.7 and 2.3 for the 40 and 130 nm bead samples, respectively. Repeated experiments show that the coefficient of variation in the magnetic susceptibility peak height of a 100 pM sample is $\sim$ 4%,[16] which translates to a variation of approximately $\pm$ 0.2 and $\pm$ 0.1 in the above given average numbers, respectively. The obtained averages are in accordance with earlier findings showing that the number of immobilized beads per DNA-coil is higher for smaller beads than for the larger ones.[16] Also, a frequency upshift for the peaks can be observed upon increasing concentration of DNA-coils, especially for the 130 nm bead sample. As found earlier,[18] this phenomenon is due to preferential immobilization of the larger beads in the bead size distribution.

Figure 2a shows a TEM overview micrograph of the negative control 130 nm bead sample (absence of DNA-coils). Various types of salt precipitates (examples of these are indicated by white arrows 1, 2, and 3) and several magnetic beads (black

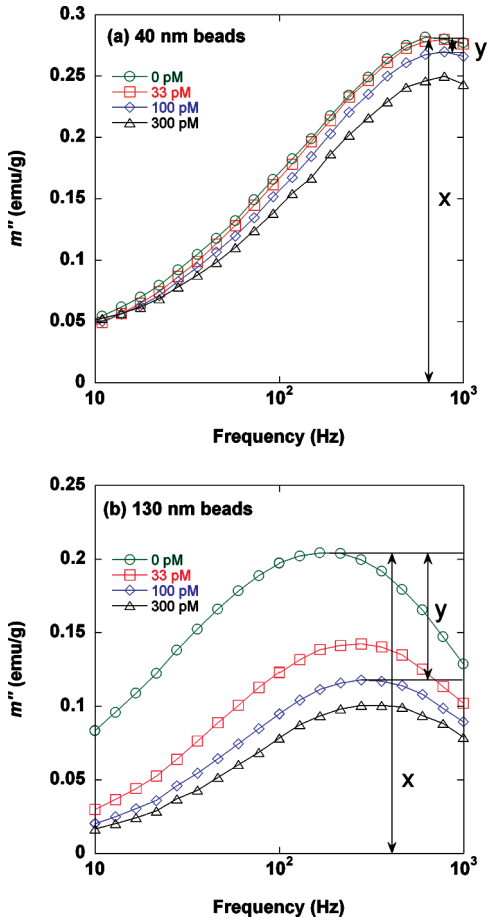

Figure 1. Imaginary part of complex magnetization (m'') vs frequency at 37 °C for samples with 40 nm beads (panel a), 130 nm beads (panel b), and various DNA-coil concentrations (0 pM to 300 pM, genomic background material included). For the samples with a 100 pM DNA-coil concentration, the total number of immobilized beads equals the total number of beads multiplied by y/x. Lines are guides for the eye.

arrow heads and highlighted in encircled area) appear on the carbon support film. The salt precipitate 1 is a circular structure with a size of ∼100 nm whereas the salt structure 2 has a square-like shape with a darker contrast than that of 1 and with a size of a few hundred nanometers and is mostly found on the flake-like structures 3 covering a big part of the substrate. A part of Figure 2a is digitally magnified (Figure 2b) to more clearly see the bead positions relative to the salt precipitates. In Figure 2a,b some examples of beads are indicated by black arrow heads. In the inset of Figure 2b, the nanostructure of an individual bead is visible. The bead is built from an irregular cluster of ∼15 nm maghemite nanoparticles (magnetic single domain grains). Therefore, the structure of the beads is distinct from the structure of the salt precipitates and can be clearly distinguished from the salt precipitates in the TEM images. Also in the bright field (BF) TEM images, the beads appear with a darker contrast than that of the salt precipitates because iron oxide has a higher elastic scattering cross-section than the salts having a lower average Z-number. In summary, the negative control sample is characterized by a wide range of salt precipitations to which some beads are linked in a random manner.

Figure 2c,d shows two TEM overview micrographs of the positive 130 and 40 nm bead samples (presence of DNA-coils), respectively. The beads in Figure 2c appear either as individuals (indicated by black arrowheads) or aggregates (indicated by black arrows) and are systematically linked in various numbers to salt precipitates. These precipitates appear now in a close to circular morphology and sizes of ∼100−400 nm on the carbon support film. Also a thread-like boundary is observed around the circular salt structures of ∼10 nm in thickness, and beads are often attached to this boundary. A large number of circular salt precipitates with or without beads are here denoted as nanostructures. Evaluation of several such nanostructures will be presented in the following text; thereby, statistically significant conclusions can be drawn. One assembly of four beads linked with one salt precipitate is indicated by a white arrowhead in Figure 2c. Figure 2d shows the same characteristic features as the positive 130 nm bead sample, and a few salt precipitates with beads are indicated by black arrows. Furthermore, the beads appear either inside or attached close to the boundary of the circular salt precipitates. The very systematic appearance of the beads in circular salt precipitations observed for both positive samples under study is not found in the negative control sample. Moreover, if the characteristic assemblies of magnetic beads observed for the positive samples were just artifacts due to drying, similar assemblies would also appear in the negative sample, which is clearly not the case. TEM methods are used by many research groups to verify nanoparticle agglomeration.[22] Thus, a reasonable interpretation is that the circular salt precipitates containing beads in the positive samples are salt residues that surround individual DNA-coils with immobilized beads. Hereafter, these circular salt spots are thus denoted as salt−DNA stains. Because of the strong negative charge of the DNA-coils, it is very unlikely that individual DNA-coils are positioned close to each other on the carbon support film. Furthermore, this interpretation is supported by the following argument and experimental findings. First, we consider the expected contrast that isolated DNA-coils would have on the carbon film. As mentioned in the Experimental Section, the total length of the 90 kbp DNA single-strand building one DNA-coil is about 30 μm. Assuming a DNA single-strand of about 1 nm thickness (width), when this strand would be spread densely as a film on a surface, the area (length multiplied by width) of the strand $A_{\text{DNA-coil}} = 0.03\ \mu\text{m}^2$. The observed average diameter of the salt−DNA stains with beads is about 0.30 μm, giving an area $A_{\text{salt-DNA-coil}}$ of about 0.07 μm^2, therefore being of similar magnitude to the area of the DNA-coil ($A_{\text{DNA-coil}}$). If we assume that the 30 μm long DNA single-strand, collapsed within this 0.30 μm disk, forms a uniform film, the height of this film is therefore around $A_{\text{DNA-coil}}/A_{\text{salt-DNA-coil}} = 0.03/0.07-0.4$ layers of DNA. From this estimation one may conclude that on most parts of the "collapsed DNA structure", the DNA strings appear individually, i.e., they are not piled up. In our experimental setup, these 0.4 layers of about 10−20 C, O, N, and P atoms on top of the 30 nm carbon support film will only result in a very faint, barely observable contrast in the TEM images. The circular nanostructure contrast observed in Figure 2c,d can therefore not be explained by the presence of DNA only. It is, thus, more reasonable to assume that the DNA-coils are visible because the buffer salts are concentrated around the DNA single-strands, which strongly increases the image contrast of the DNA-coils. Second, the formation mechanism of the collapsed DNA structures is almost completely unexplored. However, some guidance can be found in a report from Wu et al.[23] where circular DNA molecules (plasmid DNA), kept in a solution of $MgCl_2$, were deposited on mica substrates followed by drying and AFM characterization. Here, during drying, the $MgCl_2$ precipitated around the DNA molecules as measured in the AFM images. In the AFM images, the height of the combined DNA/$MgCl_2$ layer was 7 nm as compared to the about 1 nm height for a pure DNA string. In a similar way, salts are most likely collected

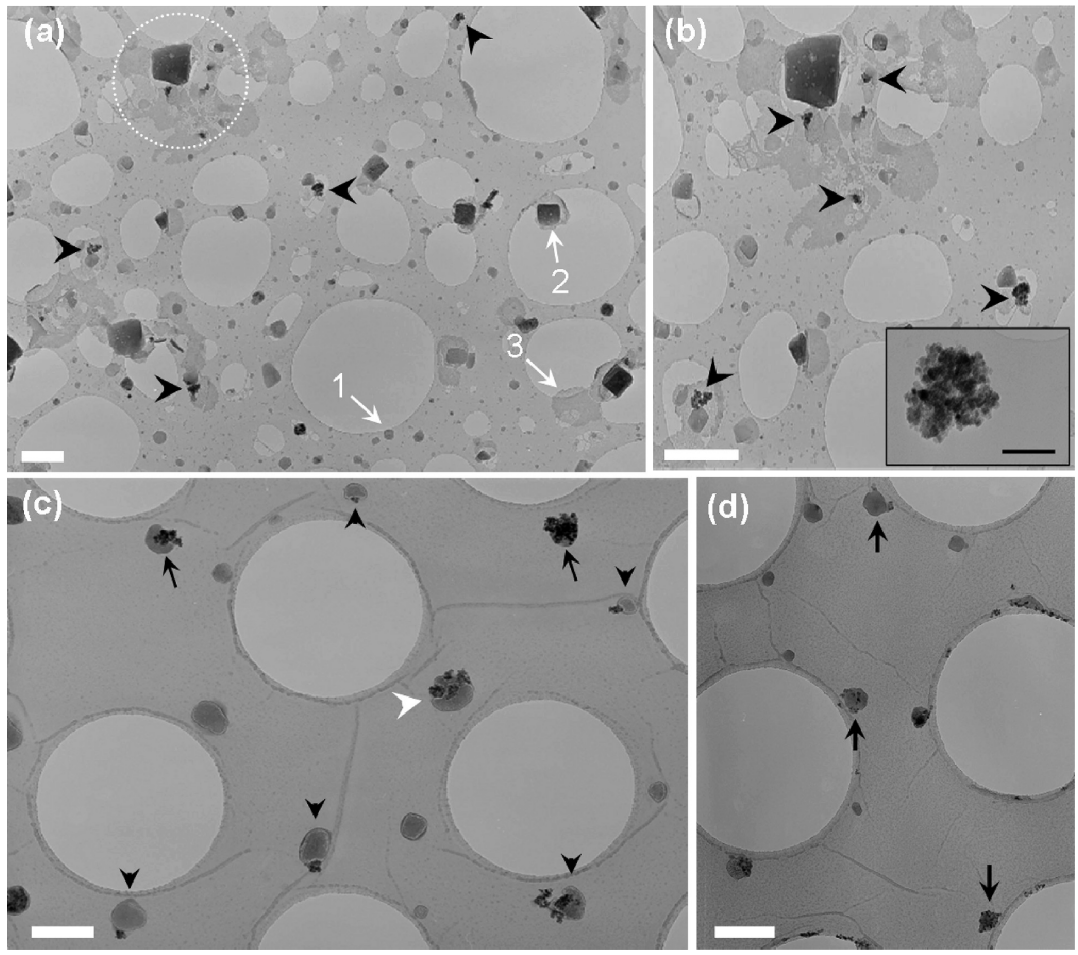

Figure 2. (a) TEM overview micrograph of a negative control 130 nm bead sample. Several morphologies of salt precipitates are observed and shown by white arrows; for instance, circular (arrow 1), square-like (arrow 2), and flake-like (arrow 3). The magnetic beads in the salt stains are indicated by black arrow heads. Some beads are highlighted by the encircled area. (b) A digitally magnified section of panel a showing the location of the beads relative to the salt stains indicated by arrow heads. The inset shows a single bead appearing close to a salt stain at high magnification. (c) TEM overview micrograph of the positive 130 nm bead sample showing several individual beads (arrow heads) and some bead aggregates attached to salt−DNA stains (black arrows). Four beads attached to a salt−DNA stain are indicated by a white arrowhead. (d) TEM overview micrograph of the positive 40 nm bead sample showing the same characteristic features as in panel c. Some salt−DNA stains containing beads are indicated by black arrows. Note that the substrate is a holey carbon film. The scale bar in the inset of panel b corresponds to 100 nm; other scale bars correspond to 500 nm.

around the DNA-coils in the positive samples of the present study during the drying process on the TEM grid. Because there is a strong electrostatic repulsion between the DNA-coils in solution, it is reasonable to assume that the bead/coil structures in the positive samples are deposited on the carbon film with a significant separation between the DNA-coils during the drying process. Also, judging from the size of the salt−DNA stains (about 100−400 nm), it is apparent that each individual DNA-coil with an approximate size of 700 nm in solution[13,20] strongly shrinks when deposited on the carbon substrate during the drying process. The explanation for this shrinkage is not clear but could possibly be related to the nature of the interaction between the DNA-strands building the coils and the carbon surface or the interaction between DNA and the salts during the drying process. This argument explains the interpretation of these circular contrasts as originating from the coprecipitation of DNA and salts.

Figure 3a,b displays high-magnification TEM micrographs of a positive 40 nm bead sample of two individual salt−DNA stains containing several beads. The inset, providing an image of the same stain as in Figure 3a acquired after 3−4 min of electron beam exposure, shows that the beads appear in four different aggregates placed mostly inside the stain boundary, which is also the case for one aggregate of 40 nm beads in Figure 3b. In contrast, in Figure 3c, showing an overview TEM micrograph from the positive 130 nm bead sample, the beads mostly appear as individuals and are found close to the boundary of the stain. In this figure, there are two stains, each containing four beads in total for which two beads in each stain are close to the center and two in each stain close to the boundaries of the stains. Furthermore, there are two stains, each containing one bead, and these beads are found on the boundaries of the stains. Figure 3d displays a salt−DNA stain in the positive 130 nm bead sample containing three individual beads of which two are on the boundary of the stain and one is inside the stain. Observations similar to those for Figure 3 are made in the entirety of the observed beads, i.e., more than 100 beads for each bead size. This observation provides some simple qualitative information about the position of beads in salt−DNA stains. In the positive 40 nm bead sample, several beads are attached to each stain and a majority of beads is located inside the salt−DNA stains. Furthermore, in stains containing several 40 nm beads, most of these beads appear in agglomerations. In contrast, for the positive 130 nm bead sample, the opposite trend is observed, i.e., most of the beads are attached on the stain boundary. As mentioned in the Experimental Section, both

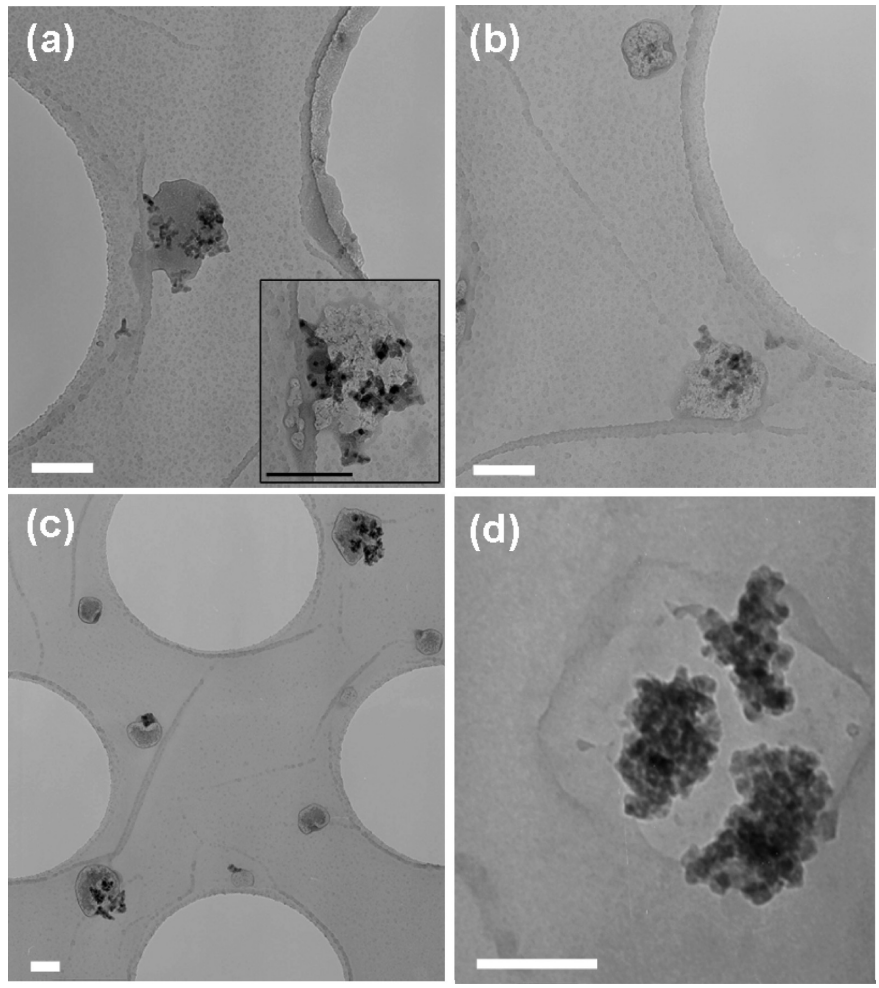

Figure 3. High magnification TEM micrographs of a positive 40 nm bead sample (a, b) and a positive 130 nm bead sample (c, d). (a, b) Overview TEM micrographs of the positive 40 nm bead sample where four aggregates of 40 nm beads are attached to one salt−DNA stain in part a and one 40 nm bead aggregate is attached to one salt−DNA stain in part b. The inset in part a shows the stain acquired after 3−4 min of electron beam exposure. (c) Overview TEM micrograph of the positive 130 nm bead sample showing that most beads appear as individuals. (d) High magnification TEM micrograph of the positive 130 nm bead sample displaying three beads attached to one salt−DNA stain. All scale bars correspond to 200 nm.

oligonucleotide-functionalized 40 and 130 nm beads appear mainly as single beads in a negative control solution, i.e., a solution containing no DNA-coils. Before attachment to the DNA-coils, the likelihood for beads to agglomerate is small because their surface is strongly negatively charged due to the oligonucleotides which give interbead repulsion. Therefore, the agglomeration in the salt stains that is observed mainly for the 40 nm beads should happen during the drying process. The model that appears from these observations is that first, in the DNA-coil, the beads are attached mainly as individual beads. When the DNA coil−salt arrangement shrinks in size during the drying process, the likelihood of neighboring bead contact increases. The fact that, for 130 nm beads, much less agglomerations are observed than for the 40 nm beads could be related to that the 130 nm beads are predominantly attached to the surface of the DNA-coils. This is observed in the images where the 130 nm beads predominantly attach to the boundary of the salt stains, whereas the agglomerates of 40 nm beads have their largest part inside the salt stains. Thus, after the drying process, the distance between many of the 130 nm beads will be long enough to not agglomerate. But in the case of the 40 nm beads, because of their small size, the likelihood of penetration into the DNA-coils is higher. Therefore, their mean distance to each other is smaller and the probability to agglomerate during the drying process is higher. This model could explain why 40 nm beads are more frequently observed in agglomerations on the salt−DNA stain compared to 130 nm beads. Both the 40 and 130 nm beads observed appear irregular in shape and exhibit some variations in size, the variation being larger for the smaller beads. The average diameters estimated from TEM micrographs of 40 and 130 nm beads (seven individual beads were considered in each case) were 45 and 135 nm, respectively; TEM micrographs are included in Supporting Information, Figure S2. The observed structural changes of stains at higher electron irradiation doses, as shown in the inset of Figure 3a, indicate the presence of organic salts and DNA in the stains.

Before analyzing the attachment of beads to salt−DNA stains quantitatively, it is important to evaluate the morphology of the salt−DNA stains. For dried salt−DNA stains that have a typical diameter of 200−300 nm (2−3 times smaller than the hydrodynamic diameter of the DNA-coils in solution), we have estimated a thickness on the order of 15 to 22 nm (details are given in Supporting Information). Though, depending on the density of the salt matrix, the thickness may differ from the calculated value, the salt−DNA stains are certainly thinner than 50 nm and appear therefore as rather flat objects with a height to width aspect ratio on the order of 1/10. Therefore, in the dried salt−DNA stain, the stain thickness is smaller or equal to the diameter of the 40 and 130 nm beads. The flatness of the

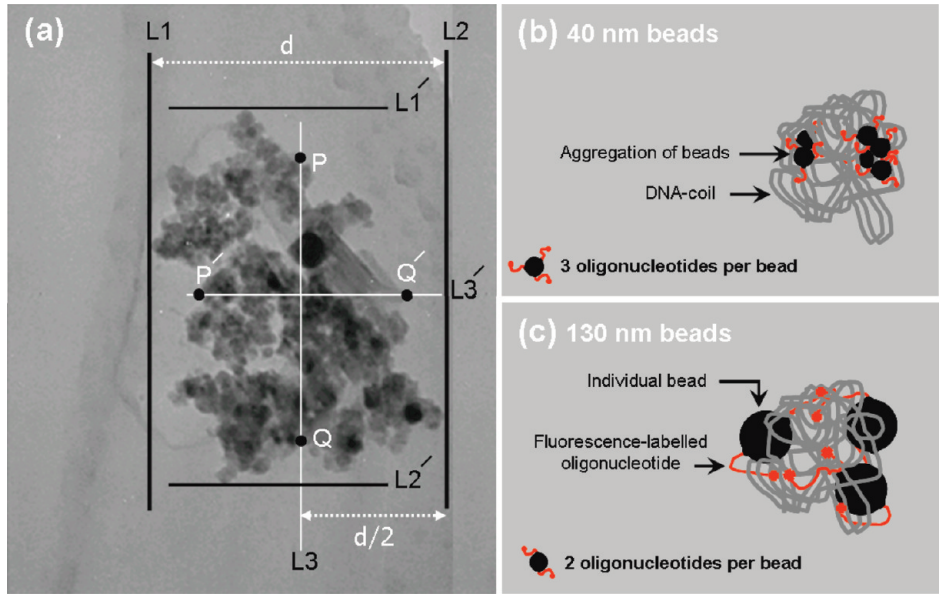

Figure 4. (a) Geometrical construction for estimation of the number of beads in a bead agglomeration (object) attached to a salt−DNA stain. Here L1 (L1′) and L2 (L2′) are the two vertical (horizontal) lines (bold black) along the outermost parts of the object boundary used to define the extension in the horizontal (vertical) direction of the object. L3 (L3′) (thin white line) is drawn at half distance between L1 and L2 (L1′ and L2′). The two points, P (P′) and Q (Q′), define the intercept between L3 (L3′) and the object boundary. The radius, R, of the object is thus defined as $R = (PQ + P'Q')/4$, and the number of beads, N, in the object can be estimated as $(R/r)^2$ rounded to the nearest integer and never less than 1, where r is the average radius of one bead. (b, c) Schematic representations of typical arrangements of 40 nm (b) and 130 nm beads (c), respectively, immobilized in DNA-coils as found by the TEM measurements.

salt stains makes it likely that, in bead agglomerations such as those observed in Figure 2, the beads order parallel to the surface of the carbon support film in a nearly two-dimensional arrangement.

As many of the observed beads appear in large irregular aggregates, we have chosen the following procedure for estimating the size of such aggregates and consequently to obtain the number of beads in every aggregate. The procedure is illustrated in Figure 4a, displaying the geometrical analysis of one salt−DNA stain containing 130 nm beads as follows: Draw two vertical lines L1 and L2 (bold black) that are tangents to the outermost boundary points of the selected object and measure the distance L1L2 = d. Draw a third vertical line, L3 (thin white), centered between L1 and L2. Identify the two points, P and Q, where L3 intercepts the boundary of the object and measure the distance PQ. Proceed accordingly for the horizontal direction, creating the horizontal lines L1′ and L2′, to obtain the line segment P′Q′. The area of the object is then defined as the area of a circle having a radius of $R = (PQ + P'Q')/4$. If r is the average radius of one bead, the number of beads in the object, N, can be estimated as $(R/r)^2$. We followed this bead counting procedure for a large number of salt−DNA stains containing beads and/or aggregates of beads, thereby obtaining the distribution of the number of beads per salt−DNA stain. In the TEM analysis, the number of analyzed salt−DNA stains containing beads was 22 and 43 for the positive 40 and 130 nm bead samples, respectively, and the total number of beads counted in salt−DNA stains was 133 and 110 for the 40 and 130 nm bead samples, respectively. From this, the average number of beads per salt−DNA stain was calculated to 6.0 ± 0.8 and 2.6 ± 0.2 for the positive 40 and 130 nm bead samples, respectively. These values are in very good agreement with the magnetic measurements (5.7 ± 0.2 and 2.3 ± 0.1 beads per DNA-coil, respectively). This means that our TEM method is reliable for analyzing the number of attached magnetic beads in DNA-coils.

Our TEM method does not provide a strict determination of bead positions in DNA-coils in the liquid samples. Thus, the observations of bead positions in salt−DNA stains made above only give indications of the qualitative character of how the beads were originally positioned in the DNA-coils before drying. Nevertheless, the smaller and the larger beads are clearly positioned differently compared to each other in the salt−DNA stains. The above observations that the aggregates of 40 nm beads are mostly turned in an inward direction with respect to the salt−DNA stains is coherent with the hypothesis that the 40 nm beads appear as unconnected beads bound partially at sites inside the DNA-coils. The preferential binding of the 40 nm beads *inside* the DNA-coils in solution supports the previous hypothesis[16,18] that positive samples containing 40 nm beads mainly consist of separate, unaggregated coils because there are only few beads on the coil boundaries that could link several coils together. Further, the observations support that 130 nm beads, because of their larger size, prefer to bind closer to the exterior of the DNA-coils in solution, which has been hypothesized by Zardán Gómez de la Torre et al.[18]

Figure 4b (40 nm beads) and 4c (130 nm beads) schematically illustrates the bead immobilization as found in the present TEM study of dried bead/DNA-coil structures. Panel b shows that 40 nm beads (three oligonucleotides per bead) preferentially appear inside the salt−DNA stains as aggregates with an average number of six beads per coil. In panel c, it is indicated that 130 nm beads (two oligonucleotides per bead) most frequently are found close to the boundary of the salt−DNA stains and appear mostly as individuals with an average number of three beads per coil.

The TEM images in Figure 2−4 are a representative selection from our data. We have counted the number of beads in a large number of salt−DNA stains containing beads. Figure 5 shows histograms of the frequency with which a specific number of beads (40 and 130 nm bead positive samples in panel a and b, respectively) in a salt−DNA stain (event) in the positive samples

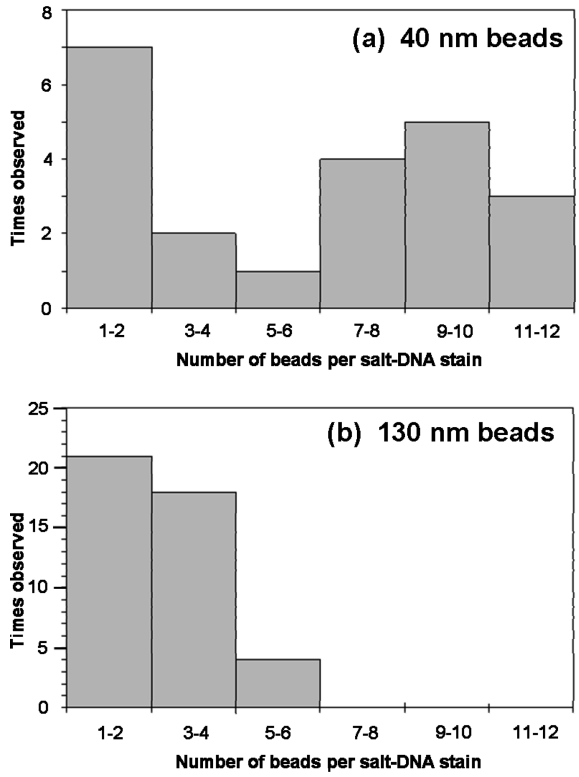

Figure 5. Distribution of the number of beads counted per salt−DNA stain (plotted with two bins) in the positive 40 nm (panel a) and 130 nm (panel b) bead samples.

is observed. Despite that there are about 10^4 times more 40 nm beads than DNA-coils (i.e., coil to bead ratio is 1:10000, see Supporting Information) and theoretically there are roughly 10^3 bead binding sites per DNA-coil, the maximum number of 40 nm beads per coil observed is only 12 (panel a). Clearly, there are certain factors that limit the bead immobilization. First, because of the collapse of the long DNA single-strand into a random-coil, it is reasonable to assume that this geometrical constraint strongly reduces the available binding sites for the beads compared to the situation when the DNA strand is completely stretched. Second, the electrostatic bead−coil repulsion could be another limiting factor for bead immobilization to DNA-coil. Third, the structure of the DNA-coil could possibly become increasingly more rigid as beads hybridize to the coil, which could make it increasingly more difficult for the beads to penetrate into the coils and bind inside. Obviously, these issues need further investigations, which are out of the scope of this paper. The observation that 130 nm beads bind in smaller amounts per DNA-coil, i.e., only a maximum of six beads (see panel b), could possibly be explained by the comparably larger size of these beads that renders them less capable of binding inside the DNA-coils. An additional explanation for why the 130 nm beads are immobilized in amounts lower than that of the 40 nm beads is that the coil to bead ratio is higher in the 130 nm bead sample (about 1:6, see Supporting Information). In Figure 5a, a bimodal distribution of the number of 40 nm beads in the DNA-coils seems to appear. Although the figure indicates that there are more DNA-coils containing 7−12 beads than 5−6 beads, we choose to omit a deeper discussion of this observation without having stronger proof.

After observation of a large number of salt−DNA stains, we could not observe any event that could point to two or more salt−DNA stains that are cross-linked through magnetic beads. Supposing that the drying process does not change the spatial arrangement of two or more possible cross-linked DNA-coils, this observation indicates that the beads do not cross-link DNA-coils. Cross-linking of DNA-coils is, in fact, not expected at the very low oligonucleotide coverage on the beads used in these experiments.[18]

4. Summary and Conclusions

In this paper, the immobilization of oligonucleotide-functionalized magnetic beads of two different sizes (40 and 130 nm) and low oligonucleotide surface coverage (three and two oligonucleotides per beads, respectively) in DNA-coils was studied by TEM. This study provides the first electron microscopy study on composites of magnetic nanoparticles and random-coiled DNA structures. In view of the large number of studies on functionalized nanoparticles, involving complex salt solutions, the pathway developed and demonstrated here can be used more generally to study the interaction between functionalized nanoparticles and their solution environment. Moreover, the findings from this study strongly increases the understanding of the underlying physicochemical mechanisms in the VAM-NDA biosensor method.

Briefly, oligonucleotide-functionalized magnetic beads and DNA-coils were mixed and after incubation of the mixture, a small quantity of the solution was dispersed on a holey carbon TEM grid and dried. Also, a negative control sample was prepared with composition essentially only differing by the absence of DNA-coils compared to the samples containing DNA-coils (positive samples). In the TEM observations, salt precipitations having a circular morphology and a size of a few hundreds of nanometers (corresponding to the size of an individual DNA-coil in the dry state with buffer salts attached to it) of which many contained beads in various numbers appeared in the positive samples, structures which were not found in the negative control sample. These very characteristic structures of beads and salt spots were interpreted as salt residues of individual DNA-coils (denoted salt−DNA stains) containing magnetic beads. The number of beads attached to each salt−DNA stain was analyzed for a large number of bead-containing stains for the two positive samples using a two-dimensional approach, and the results were compared with magnetic measurements on similar samples (same ratio between the number of beads and DNA-coils as in the TEM samples), providing the average number of beads per DNA-coil. A good agreement was found between the average number of 40 and 130 nm beads attached per salt−DNA stain obtained from the TEM analysis (6.0 ± 0.8 and 2.6 ± 0.2 beads per salt−DNA stain, respectively) and the average number of immobilized beads per DNA-coil extracted from magnetic measurements (5.7 ± 0.2 and 2.3 ± 0.1 beads per DNA-coil, respectively). Also, a qualitative difference in location of beads in the salt−DNA stains was observed for the 40 and 130 nm bead samples. The 40 nm beads were found closer to the center of the salt−DNA stains compared to the 130 nm beads, which mostly appeared close to the boundary of the stains. These observations were consistent with findings in previous papers (not involving electron microscopy) and supported our hypothesis that smaller beads more easily penetrate into the DNA-coils in solution, thereby preferably hybridizing in the interior of the coils, compared to larger beads which mostly hybridize on the outer boundary of the DNA-coils.

Acknowledgment. The Knut and Alice Wallenberg Foundation (KAW), the Swedish Foundation for Strategic Research (SSF), the Swedish Defence Nanotechnology program, and the

Swedish Research Council (VR) are gratefully acknowledged for their financial support. S.A. acknowledges financial support from the Higher Education Commission (HEC) of Pakistan, and S. Rubino for support of this work.

Supporting Information Available: TEM sample compositions, details of thickness estimation of salt−DNA stains, and TEM micrographs lying behind the estimation of bead mean sizes. This material is available free of charge via the Internet at http://pubs.acs.org.

References and Notes

(1) Yager, P.; Edwards, T.; Fu, E.; Helton, K.; Nelson, K.; Tam, M. R.; Weigl, B. H. *Nature* **2006**, *442*, 412.

(2) Jenison, R.; Yang, S.; Haeberli, A.; Polisky, B. *Nat. Biotechnol.* **2001**, *19*, 62.

(3) Kerman, K.; Kobayashi, M.; Tamiya, E. *Meas. Sci. Technol.* **2004**, *15*, R1.

(4) Klostranec, J. M.; Xiang, Q.; Farcas, G. A.; Lee, J. A.; Rhee, A.; Lafferty, E. I.; Perrault, S. D.; Kain, K. C.; Chan, W. C. W. *Nano Lett.* **2007**, *7*, 2812.

(5) Wang, J. *Small* **2005**, *1*, 1036.

(6) Gooding, J. J. *Small* **2006**, *2*, 313.

(7) Tamanaha, C. R.; Mulvaney, S. P.; Rife, J. C.; Whitman, L. J. *Biosens. Bioelectron.* **2008**, *24*, 1.

(8) Lee, W.; Joo, S.; Kim, S. U.; Rhie, K.; Hong, J.; Shin, K. H.; Kim, K. H. *Appl. Phys. Lett.* **2009**, *94*, 153903.

(9) Wang, S. X.; Li, G. *IEEE Trans. Magn.* **2008**, *44*, 1687.

(10) Connolly, J.; St Pierre, T. G. *J. Magn. Magn. Mater.* **2001**, *225*, 156.

(11) Astalan, A. P.; Ahrentorp, F.; Johansson, C.; Larsson, K.; Krozer, A. *Biosens. Bioelectron.* **2004**, *19*, 945.

(12) Mondi, C.; Leifer, K.; Mavrocordatos, D.; Perret, D. *J. Microsc.* **2002**, *207*, 180.

(13) Strömberg, M.; Göransson, J.; Gunnarsson, K.; Nilsson, M.; Svedlindh, P.; Strømme, M. *Nano Lett.* **2008**, *8*, 816.

(14) Svedlindh, P.; Gunnarsson, K.; Strömberg, M.; Oscarsson, S. Bionanomagnetism. In *Nanomagnetism and Spintronics- Fabrication, Materials, Characterization and Applications*; Nasirpouri, F., Nogaret, A., Eds.; World Scientific Publishing: Singapore, 2009.

(15) Strömberg, M.; Gunnarsson, K.; Valizadeh, S.; Svedlindh, P.; Strømme, M. *J. Appl. Phys.* **2007**, *101*, 023911.

(16) Strömberg, M.; Zardán Gómez de la Torre, T.; Göransson, J.; Gunnarsson, K.; Nilsson, M.; Strømme, M.; Svedlindh, P. *Biosens. Bioelectron.* **2008**, *24*, 696.

(17) Strömberg, M.; Zardán Gómez de la Torre, T.; Göransson, J.; Gunnarsson, K.; Nilsson, M.; Svedlindh, P.; Strømme, M. *Anal. Chem.* **2009**, *81*, 3398.

(18) Zardán Gómez de la Torre, T.; Strömberg, M.; Russell, C.; Göransson, J.; Nilsson, M.; Svedlindh, P.; Strømme, M. *J. Phys. Chem. B* **2010**, *114*, 3707.

(19) Strömberg, M.; Gunnarsson, K.; Johansson, H.; Nilsson, M.; Svedlindh, P.; Strømme, M. *J. Phys. D: Appl. Phys.* **2007**, *40*, 1320.

(20) Melin, J.; Jarvius, J.; Gransson, J.; Nilsson, M. *Anal. Biochem.* **2007**, *368*, 230.

(21) Dahl, F.; Baner, J.; Gullberg, M.; Mendel-Hartvig, M.; Landegren, U.; Nilsson, M. *Proc. Natl. Acad. Sci. U.S.A.* **2004**, *101*, 4548.

(22) El Khoury, J. M.; Caruntu, D.; O' Connor, C. J.; Jeong, K. U.; Cheng, S. Z. D.; Hu, J. *J. Nanopart. Res.* **2007**, *9*, 959.

(23) Wu, A. G.; Li, Z.; Zhou, H. L.; Wang, E. K. *Superlattices Microstruct.* **2005**, *37*, 151.

JP105756B